

## Reduced Turbine Emissions Using Hydrogen-Enriched Fuels

**R.W. Schefer**

Combustion Research Facility  
Sandia National Laboratories  
Livermore, CA 94551-0969

### ABSTRACT

The stability characteristics of a prototype premixed, hydrogen-fueled burner were studied. The potential application is the use of hydrogen as a fuel for aircraft gas turbine operation. The burner configuration consisted of nine 6.73 mm diameter channels through which the reactants entered the burner. Hydrogen was injected radially inward through small diameter holes located on opposite sides of each air channel. In this way the region over which hydrogen and air were premixed was minimized to prevent potential flashback problems. Flame stability was studied over a range of fuel-lean operating conditions since lean combustion is currently recognized as an effective approach to NO<sub>x</sub> emissions reduction. In addition to pure hydrogen and air, mixtures of hydrogen-blended methane and air were studied to evaluate the potential improvements in flame stability as hydrogen replaces methane as the primary fuel component.

### INTRODUCTION

The development of advanced combustion capabilities for gaseous hydrogen and hydrogen-blended hydrocarbon fuels in gas turbine applications is an area of much current interest. Driving this interest are several current needs. One need is the cost-effective utilization of alternative fuels with a wide range of heating values. For example, low and medium heating value fuels containing significant hydrogen are often produced as a by-product in Coal-Gasification Combined Cycle and Fluidized Bed Combustion installations. These product gases could provide a significant source of cost-effective fuels for gas turbines. A second need is related to the recognition that ultra-lean premixed combustion is an effective approach to NO<sub>x</sub> emissions reduction from gas turbine engines. Hydrogen blended with traditional hydrocarbon fuels significantly improves flame stability during lean combustion and allows stable combustion at the low temperatures needed to minimize NO<sub>x</sub> production. A longer-term need is the desire to eliminate UHC and CO<sub>2</sub> emissions. The use of hydrogen-blended hydrocarbon fuels provides both a solution to the immediate need for NO<sub>x</sub> reduction, and also provides a transition strategy to a carbon free energy system in the future.

Changes in fuel composition, particularly the addition of hydrogen to hydrocarbon fuels, affect both the chemical and physical processes occurring in flames. These changes affect flame stability, combustor acoustics, pollutant emissions, combustor efficiency and other important quantities. Few of these issues are clearly understood. Studies in the literature related to the use of hydrogen as both the primary fuel and a fuel additive have been directed toward the

effects of small amounts of hydrogen addition on hydrocarbon flame stability and pollutant formation under fuel-lean conditions. For example, studies in spark ignition engines clearly show the benefits of hydrogen blended with natural gas on exhaust emissions (Larson and Wallace, 1997) and on extending the lean engine operating limits (Meyers and Kubesh, 1997; Bell and Gupta, 1997). Early results in large-scale gas turbine combustors also indicate advantages to hydrogen addition. Clayton (1976) carried out a study on the effect of hydrogen addition in aircraft gas turbines. Up to 15% hydrogen addition to JP-5 or JP-6 produced leaner blowout limits and corresponding reductions in  $\text{NO}_x$  (less than 10 ppm @ 15%  $\text{O}_2$ ) while maintaining acceptable CO and HC emissions levels. Anderson (1975) premixed hydrogen with propane (up to 5% of the total fuel flow) to show that  $\text{H}_2$  addition extended the premixed lean flammability limits and improved combustion efficiency. These tests were carried out at reactant inlet temperatures up to 700K and pressures up to 5 atm. In a subsequent study (Anderson, 1976), experiments using premixed hydrogen and air demonstrated  $\text{NO}_x$  emission levels of 0.06 ppm and combustion efficiency of 98% at an equivalence ratio of 0.24. Tests conducted in a single combustor test stand at full pressure and temperature at the GE Corporate Research and Development Center demonstrated improved flame stability with hydrogen addition to natural gas fuel (Morris et al., 1998). Blends of up to 10% hydrogen by volume showed reduced CO emissions with increased hydrogen addition under lean conditions, and lower  $\text{NO}_x$  emissions for a given CO level.

At a more fundamental level, the results of stretched flame calculations at elevated pressure (30 atm) (Gauducheau et al., 1998) showed that the improved lean flame stability was attributed to hydrogen's higher flame speed and increased resistance to strain. It was further noted that flame radical concentrations (O, H and OH) increased significantly with hydrogen addition in strained flames. These observations are consistent with the speculations of Phillips and Roby (1999) who attributed the enhanced reaction rates with hydrogen to an increase in the radical pool.

The objective of the present work is to evaluate the stability characteristics of a prototype fuel-lean, premixed burner designed for use with hydrogen as a fuel. This burner was developed by Dr. T. D. Smith and Dr. C. J. Marek under the Zero  $\text{CO}_2$  Program at NASA Glenn. The long-term emphasis is on the use of pure hydrogen. However, results using mixtures of hydrogen blended with methane are also presented in an effort to extend previous literature studies that considered the addition of only small amounts (typically less than 20% by volume) of hydrogen to hydrocarbon flames.

## EXPERIMENTAL SYSTEM

### Burner Description and Flow Conditions

The burner apparatus is shown in Fig. 1. The burner configuration consists of nine 6.73-mm (0.265") diameter holes, or channels, in a base plate through which the reactants enter the burner combustion section. Pure air enters the channels through the back plane of the base plate, while hydrogen is injected radially inward through two 0.894-mm (0.0352") diameter holes located on opposite sides of each air channel. In this way, the region over which hydrogen and air are premixed is minimized to prevent potential flashback problems. A 1-m straight length of 38-mm (1.5") diameter pipe upstream of the base plate provides a fully-turbulent airflow. The confinement section of the combustor is provided with four flat quartz windows that provide optical access for visual observation and for the application of laser-diagnostics. Combustion air is provided by an air compressor and metered upstream of the burner using mass flow meters for flow rates up to 2000 slm. The air is dried and filtered to remove particles by suitable

in-line filters. The fuels, methane and hydrogen, are metered using mass flow meters. The mass flow meters are calibrated using laminar flow elements to an estimated accuracy of 2%.

a)



b)



**Fig. 1.** NASA burner. a) Reactant inlet manifold (left) and windowed burner confinement section (right). b) Close up view of reactant inlet and H<sub>2</sub> radial injection holes.

### OH Fluorescence Imaging

A frequency-doubled, Nd:YAG-pumped dye laser provided the ultraviolet laser radiation for excitation of the OH molecule. The beam (8-ns pulse duration,  $0.3\text{-cm}^{-1}$  line width) was used to pump the  $Q_1(8)$  line of the (1,0) band of the OH  $A^2\Sigma - X^2\Pi$  electronic transition at 283.556 nm. Excitation from the  $N''=8$  level was selected to minimize the temperature sensitivity of the fractional population within the absorbing level. The laser-pumped  $Q_1(8)$  line has a population fraction that varies by only 10 percent over the temperature range 1000 K to 2300 K. The OH fluorescence signal was collected using a 105-mm focal length, f/4.5 UV Nikkor lens, passed through a Schott WG305 colored glass filter, and focused onto an intensified CCD camera. The intensifier was gated for 400 ns, encompassing the 8-ns laser pulse, to minimize the effects of flame luminescence and background light. The camera was operated in a 512 x 512-pixel format. With a magnification of 0.15, each image provides a field-of-view of 81.9 mm x 81.9 mm with a spatial resolution of 160  $\mu\text{m}/\text{pixel}$ .

Each OH image was normalized by the measured laser sheet intensity distribution and corrected for variations in pulse energy on a shot-by-shot basis. Corrections were made to the images for variations in camera pixel sensitivity (flatfield) and background scattered light. Under the current flame conditions, with the pumping and detection scheme used, the OH fluorescence signal can be interpreted as the OH mole fraction to within 20 percent.

### **Experimental Results**

The flame stability characteristics were determined for the burner over a range of operating conditions. The main parameters studied were the inlet flow rate, or velocity, and the overall fuel/air equivalence ratio,  $\Phi$ . In all results described below, the inlet flow rate used is the total combined flow rate of air and fuel. The inlet flow velocity,  $u$ , is then based on this total flow rate and the total area of the nine 6.73-mm diameter inlet flow channels. An additional parameter, the mole fraction of  $\text{H}_2$  in the fuel mixture,  $n_{\text{H}_2} = \text{moles H}_2 / (\text{moles H}_2 + \text{moles CH}_4)$ , was added as a flow variable. This provided control over the flame speed, which is significantly reduced by the addition of small amounts of  $\text{CH}_4$ . This variable also provides the possibility of studying the effect of flame speed variations on the flame characteristics and evaluating potential improvements in stability under conditions where hydrogen is the primary fuel component.

### Flame Stability

Flame stability was characterized in flames varying amounts of  $\text{H}_2$  addition. Figure 2 shows blowout curves for values of  $n_{\text{H}_2} = 0.7, 0.8, 0.9$  and 1.0. Note that only fuel lean conditions were studied since fuel lean combustion is the likely method of  $\text{NO}_x$  control in future gas turbine combustors. These measurements were obtained by igniting the flame at near stoichiometric conditions ( $\Phi = 0.9$ ) and then, with a constant total (fuel+air) flow rate (or inlet velocity), decreasing the fuel/air ratio until the flame completely extinguishes, or blows out. The flame typically becomes unstable with visible oscillations in its size and location as the blowout condition is approached. The increase in hydrogen content from 70% to 100% results in a significant shift in flame blowout conditions to leaner fuel/air ratios. This shift is consistent with studies in the literature showing an increase in the lean flammability limits with the addition of small amounts (<40%) of hydrogen to methane (Schefer et al., 2002) and verifies that  $\text{H}_2$  addition significantly extends lean flame stability even at the higher percentages considered here. For example, at a velocity of 60 m/s, increasing  $n_{\text{H}_2}$  from 0.7 to 1.0 reduces the equivalence ratio at flame blowout from  $\Phi = 0.40$  to 0.12.

During the measurement of the flame stability maps different flame regimes could be identified. These more detailed regimes are shown in Fig. 3 for  $n_{H_2}=0.8$ . The points labeled a, b and c at  $u=30$  m/s correspond to each of the three flame regimes identified. Shown in Fig. 4 are flame emission photographs corresponding to these flames. At the highest equivalence ratio (Fig. 4a), multiple stable lifted flames are observed. For each reactant channel, a separate flame can be identified, although the outer portions of the individual flames do overlap. The flame liftoff height is about 20 mm above each reactant channel and the flame luminescence extends over a distance of about 43 mm. Each flame appears stable, with little axial or radial movement observed visually. Note that there is some temporal averaging due to the finite time response of the eye, so the instantaneous structure and location of the flames could vary significantly from what is observed visually. No flame luminescence is seen extending above the end of the confinement section, indicating a relatively short reaction zone. As the equivalence ratio is reduced (Fig. 4b), a region of unsteady lifted flames is observed. While each reactant channel again has a separate flame associated with it, the vertical location of the flame oscillates at a frequency on the order of 1 or 2 Hz. Intermittently, individual flames can be seen to closely approach the reactant channel inlet and then move downstream. The noise level also increases in this regime, with the increased noise perhaps related to interactions between the incoming reactant flow and the flame when it is located upstream near the reactant inlet.

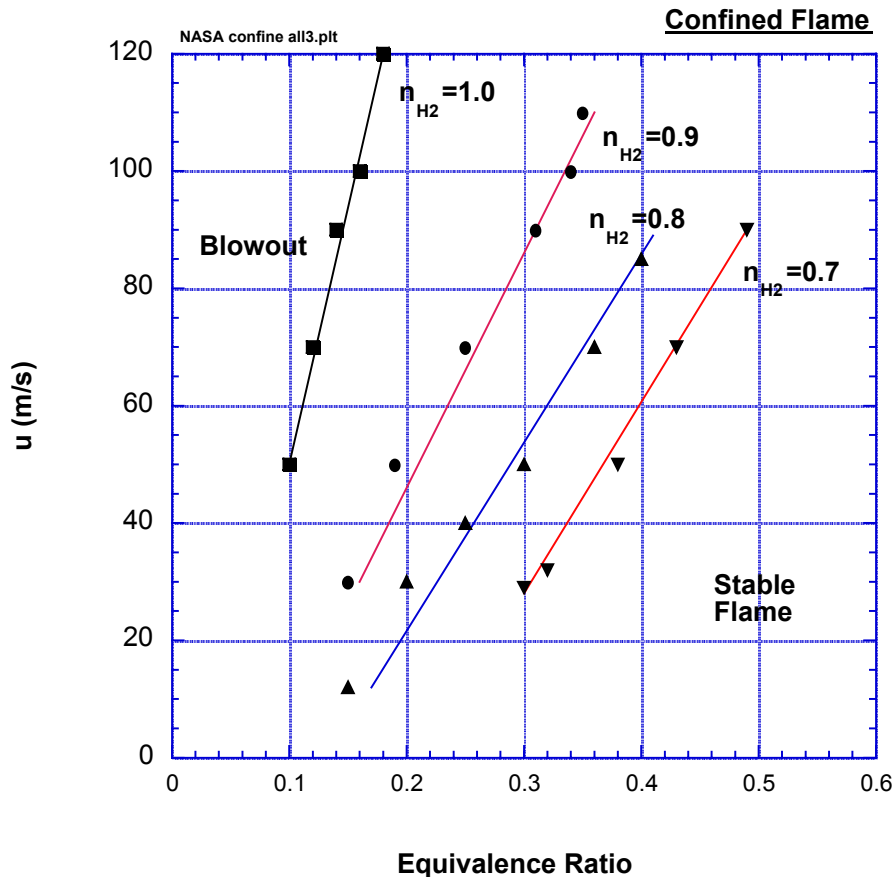
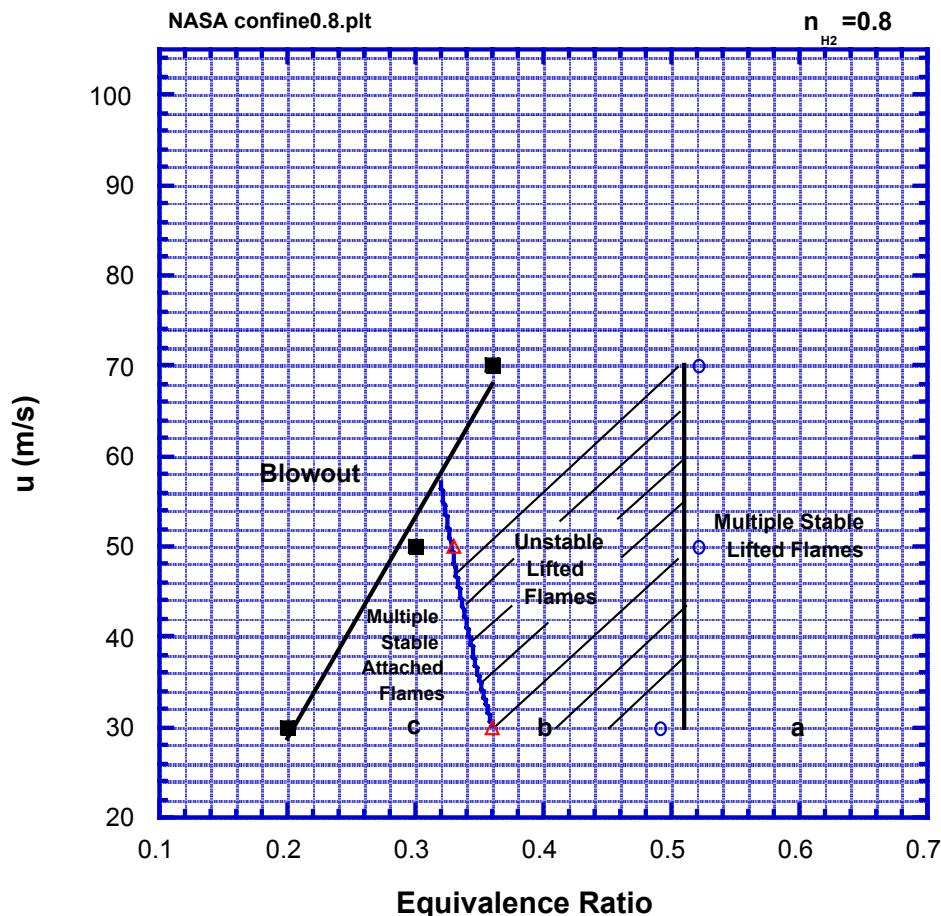
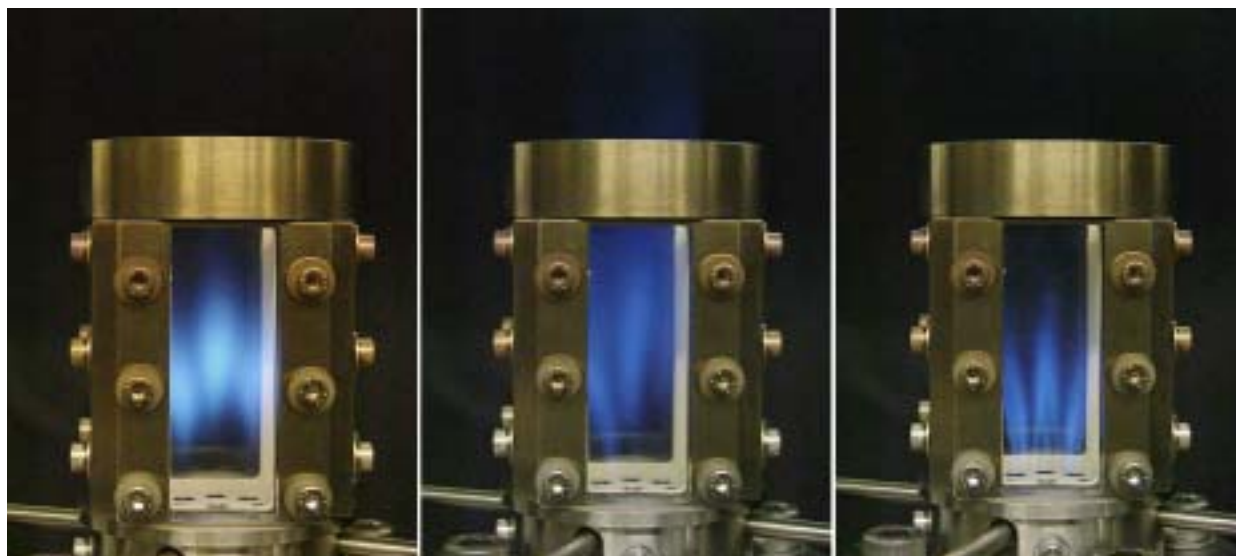


Fig. 2. Effect of hydrogen addition on burner blowout map. Confined flame.



**Fig. 3.** Detailed flame regime and stability map for  $n_{H_2}=0.8$ . Confined flame.

Further reductions in the equivalence ratio (Fig. 4c) result in each flame moving upstream and attaching at the reactant channel inlet. The typical visible flame length under these conditions is about 40 mm. These flames appear quite stable with little movement in their visually-averaged location. Further reductions in equivalence ratio lead to the sudden simultaneous blowout of the individual flames. It is interesting in Fig. 3 that these three flame regimes are readily apparent at lower inlet velocities. However, at inlet velocities above about 60 m/s, the flames no longer attach to the reactant inlet and only the stable and unstable lifted flame regimes are observed.



**Fig. 4.** Direct flame luminosity photographs for confined flame.  $n_{H_2}=0.8$ ,  $u=30$  m/s. a)  $\Phi = 0.6$ ; b)  $\Phi = 0.4$ ; c)  $\Phi = 0.3$ .

OH PLIF images corresponding to the three flames of Fig. 4 are presented in Fig. 5. Four instantaneous images from different laser shots are shown at each flame condition to illustrate the time-varying characteristics of the flow. Note that white horizontal solid lines indicate locations along the center of the burner where a solid surface exists between the inlet channels, while breaks between these lines indicate channel openings where reactants enter the combustion chamber. The images in Fig. 5a are for the highest equivalence ratio of 0.60 and clearly show that the flame is lifted between 15 mm to nearly 30 mm above the inlet plane. This liftoff height oscillates from shot-to-shot. The upstream edge of the flame (as indicated by the high OH region) is very irregular and probably reflects variations in the local velocity, which contort the flame surface. The OH is uniform throughout large regions of the downstream flame, with the highest concentration regions existing along the upstream edges of the high OH region. These high concentration regions correspond to what could be considered as the primary flame zone, which is located between the unburned reactants and the hot product gases. Recent OH PLIF measurements in rod stabilized, premixed  $CH_4$ /air flames also show peak OH levels in the primary flame zone along the interface between incoming reactants and hot combustion product gases, with a subsequent decrease downstream as radical recombination reactions lower the OH levels (Nguyen and Paul, 1996). More gradual variations in OH are seen throughout the flame in downstream regions, with only a few breaks or holes seen in the OH surface.

The OH images seen in Fig. 5b for  $\Phi = 0.40$  again show a flame that is lifted, but also present a considerably more broken, or intermittent, flame surface. This likely reflects the greater unsteadiness observed visually in this flame, with the flame stabilization location, or liftoff height oscillating in the vertical direction. This flame was also considerably more noisy. The OH images confirm large oscillations in the liftoff height as the location of the first appearance of OH varies between as little as 5 mm to nearly 30 mm downstream.

At the leanest equivalence ratio of  $\Phi = 0.30$  the flame is visually stable and attached. The corresponding OH images in Fig. 5c confirm this, with two OH regions extending upstream from the main flame zone to the solid walls located adjacent to the central channel opening. (Note that blocking of the camera by the frame around the window results in no signal in the region extending several millimeters above the solid walls. The OH signal extends up to the actual wall). Analogous to the flow field produced downstream of a centerbody, it is likely that recirculation zones are formed between the inlet channels and downstream of the solid walls in the plane of the laser light sheet. Velocity field measurements downstream of a centerbody show a recirculation zone that extends one to two centerbody diameters downstream, followed by a wake region with a velocity deficit near the centerline (Taylor and Whitelaw, 1984). These recirculation and wake zones provide low velocity regions that are favorable to upstream flame propagation from the larger downstream flame zone.

A nonreacting region typically extending between 30 mm and 50 mm downstream of the inlet plane is seen above the reactant inlet channel in the center of the images. This region can be characterized as a high velocity jet of premixed reactants where the velocity is too high to allow the flame to stabilize. It can also be seen that the highest OH concentration is along the interface between the nonreacting jet region and the recirculation/wake region consisting of hot product gases. Again the high OH region exhibits a more continuous sheet-like appearance rather than the largely broken surface seen in Fig. 5b.

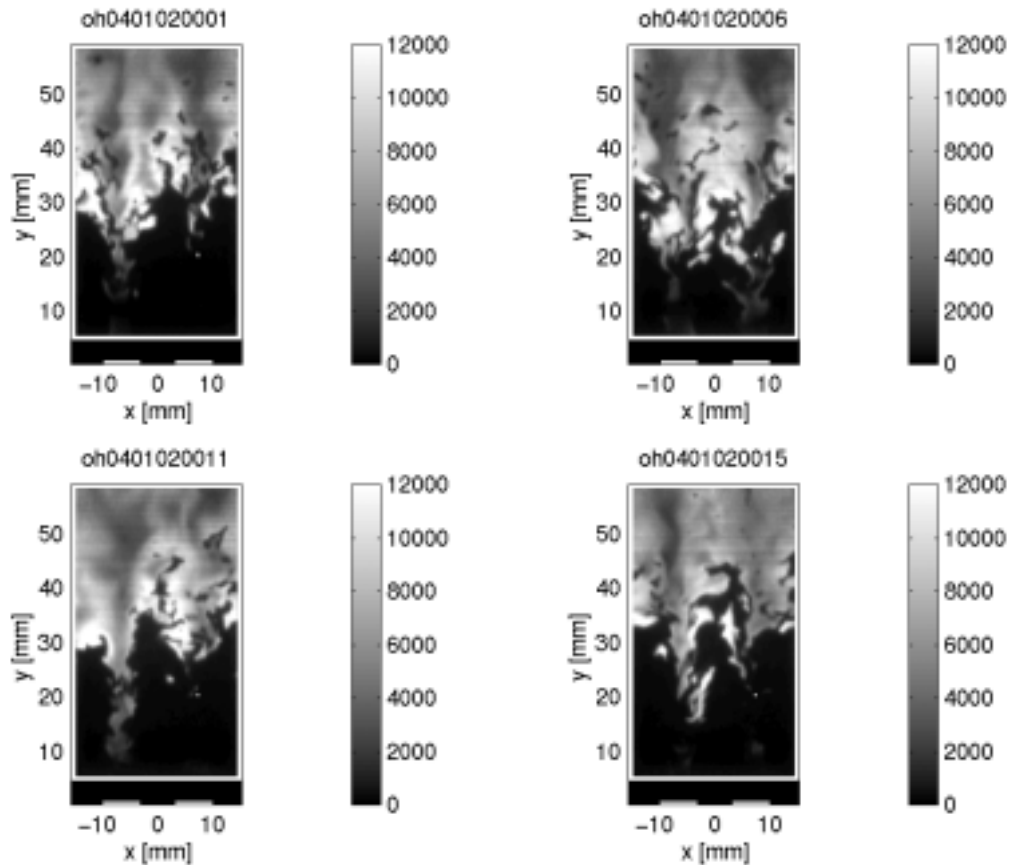


**Fig. 5a.** OH PLIF images in confined flame.  $n_{H_2}=0.8$ ,  $u=30$  m/s,  $\Phi =0.60$ .

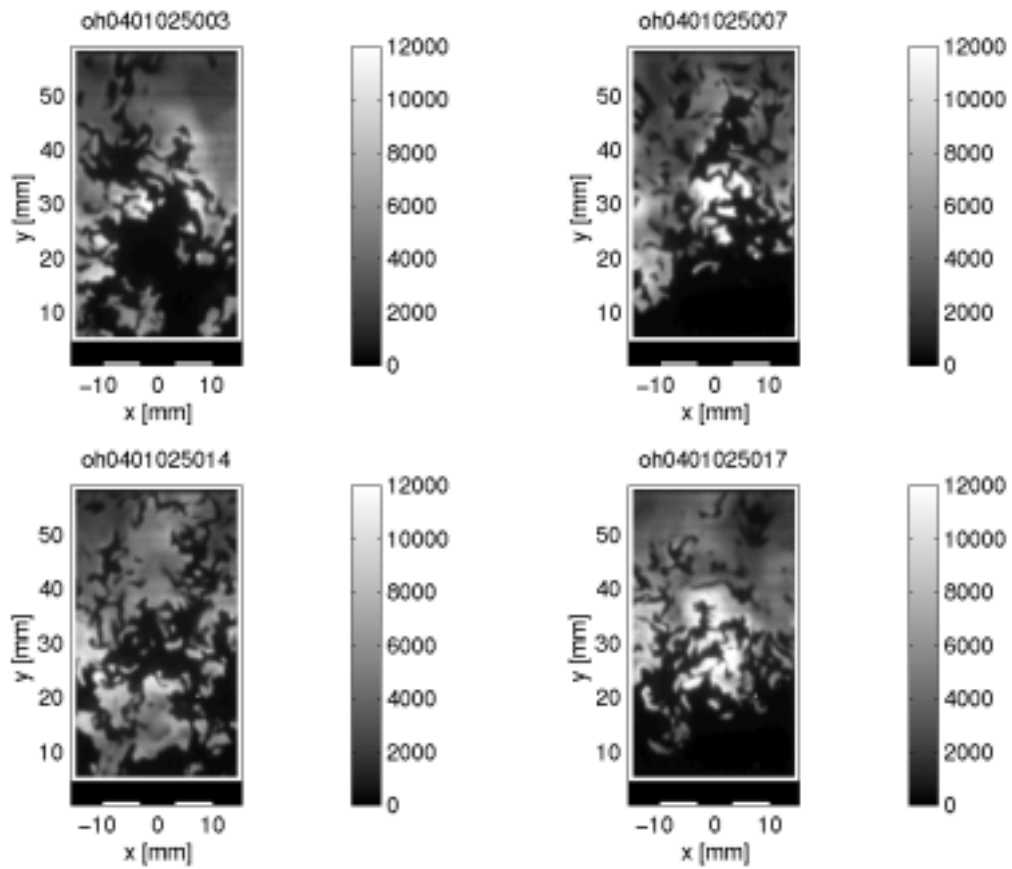


**Fig. 5b.** OH PLIF images in confined flame.  $n_{H_2}=0.8$ ,  $u=30$  m/s,  $\Phi =0.40$ .

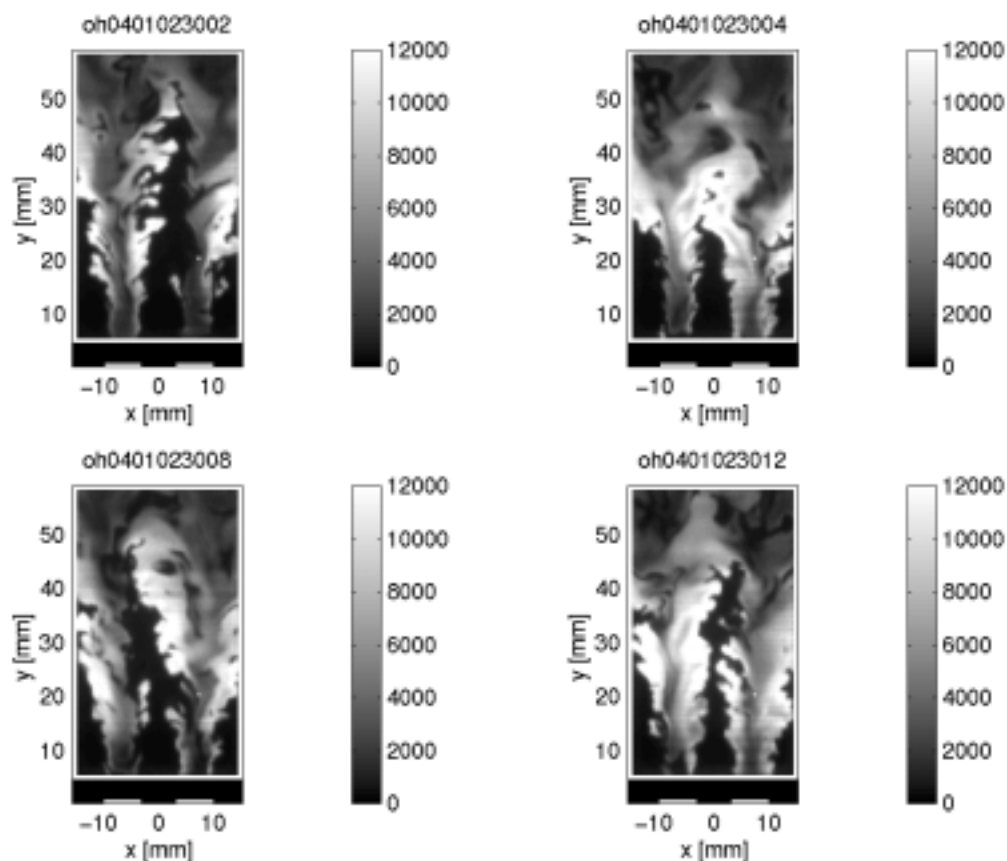


**Fig. 5c.** OH PLIF images in confined flame.  $n_{H_2}=0.8$ ,  $u=30$  m/s,  $\Phi =0.30$ .

Detailed flame regime maps were obtained for  $n_{H_2}=0.9$  and 1.0 to further explore these observed flame regimes. These are shown in Figs. 6 and 7, respectively. At both  $n_{H_2}=0.8$  and 0.9, a lower velocity region exists where flames attached to the reactant channel inlets are observed, with the maximum velocity at which an attached flame is seen increasing with increasing  $n_{H_2}$ . The detailed flame regime map for  $n_{H_2}=1.0$  in Fig. 7 exhibits somewhat different behavior. Over the velocity range investigated all flames were attached to the individual reactant inlet channels. No lifted flames were observed. This behavior is consistent with the increase in maximum velocity for the attached flame regime as  $n_{H_2}$  is increased. Thus, an unstable lifted flame regime may exist at velocities greater than the 120 m/s attained in the experiment. The points labeled a and b in Fig. 7 correspond to the two flame luminosity photographs shown in Fig.8. Both of these flames are in the multiple stable attached flame regime, with the flame in Fig. 8a corresponding to conditions nearer flame blowout. Visually, approaching blowout, the individual flames become shorter and less luminous.

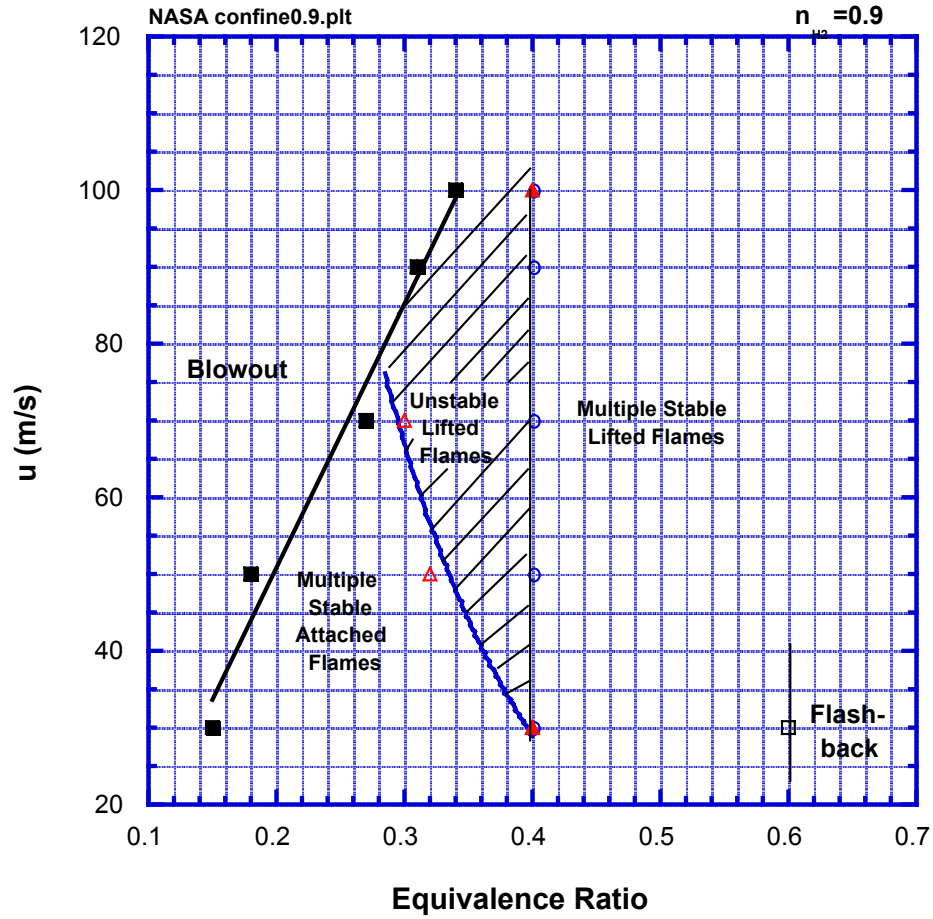


Fig. 6. Detailed flame regime and stability map for  $n_{H_2}=0.9$ . Confined flame.

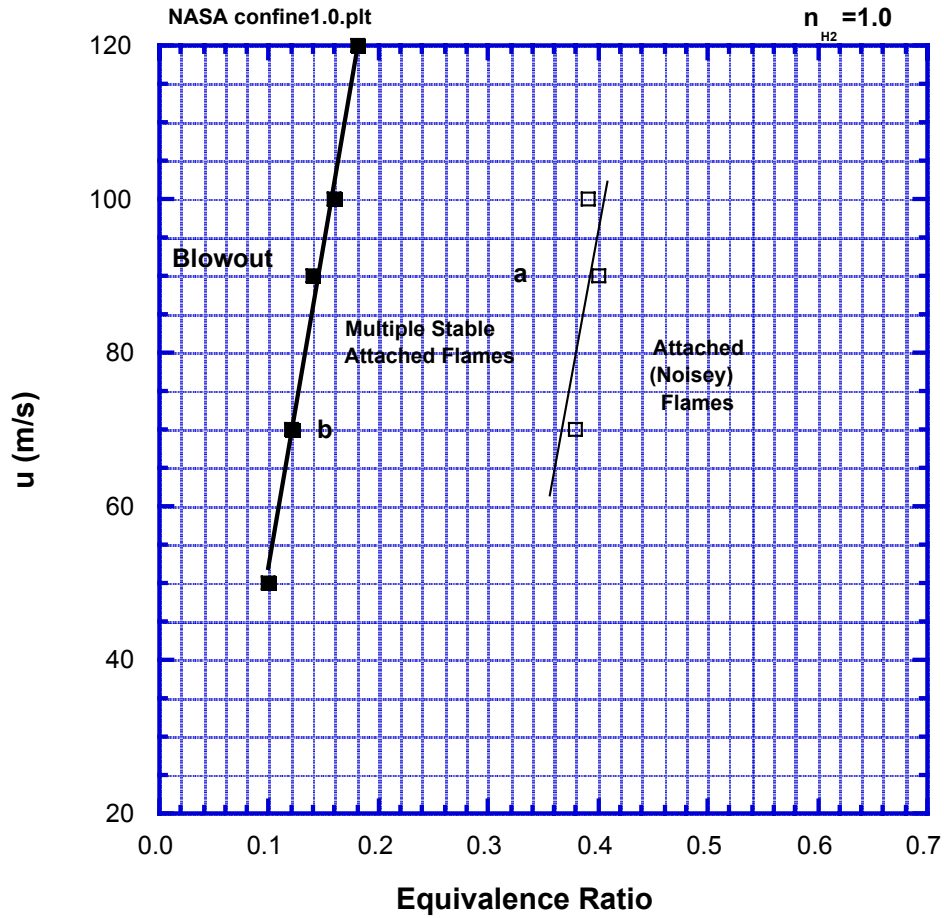
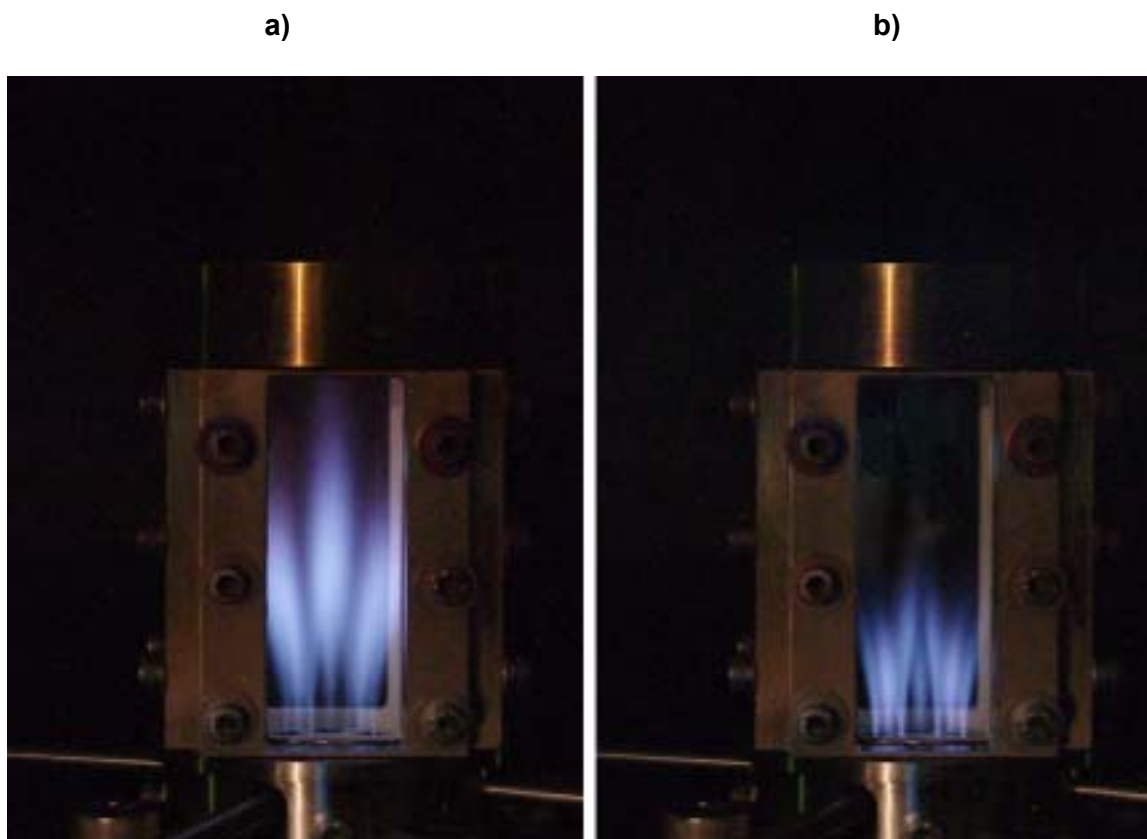


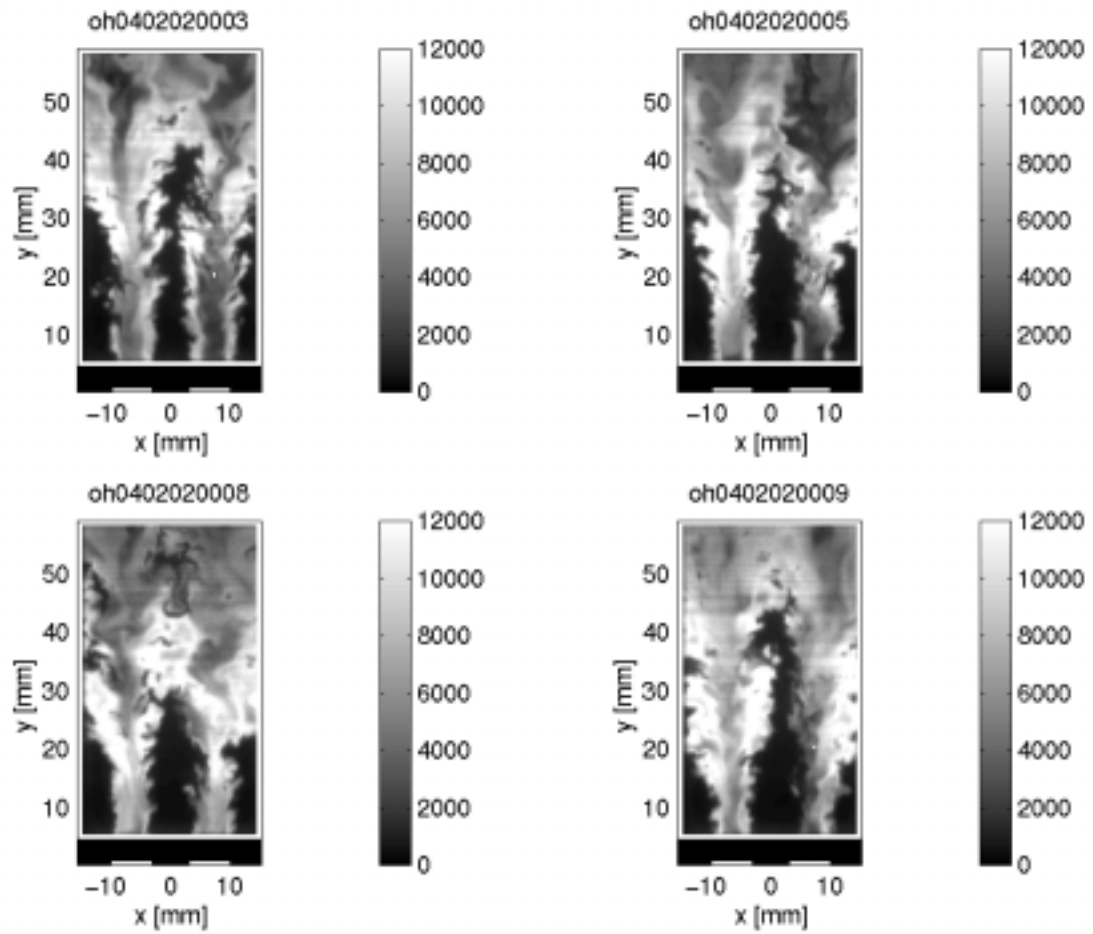
Fig. 7. Detailed flame regime and stability map for  $n_{H_2}=1.0$ . Confined flame.



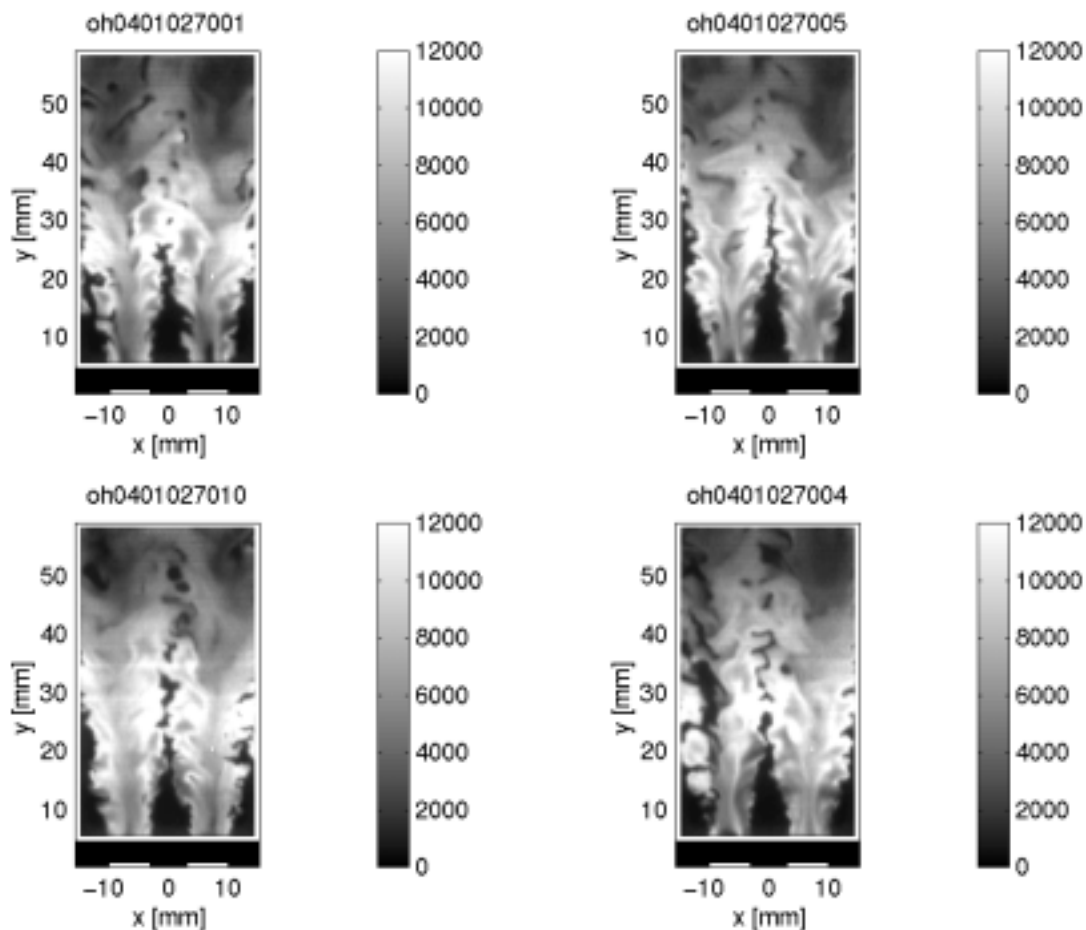
**Fig. 8.** Direct flame luminosity photographs for confined flame.  $n_{H_2}=1.0$ . a)  $u=90$  m/s,  $\Phi =0.33$ ; b)  $u=70$  m/s,  $\Phi =0.15$ .

Figure 9 shows PLIF images of the OH distribution corresponding to the flames pictured in Fig. 8. The four images in Fig. 9a are for  $n_{H_2}=1.0$ ,  $u=90$  m/s and  $\Phi =0.33$  (point a). Similar to Fig. 5c, the flame is attached to the burner surface, with the high OH region extending upstream to the solid surfaces adjacent to the reactant inlet channels. A nonreacting, high velocity jet region typically extending between 30 mm and 50 mm downstream of the inlet plane is also seen above the reactant inlet channel in the center of the images. The highest OH concentrations are found along the vertical interfaces between the nonreacting jet region and the reacting recirculation/wake region. The OH images in Fig. 9b for  $n_{H_2}=1.0$ ,  $u=70$  m/s and  $\Phi=0.15$  (point b) are similar with the exception that the nonreacting jet region does not extend as far downstream as in Fig 9a. This observation would seem to confirm the speculation that this region can be characterized as a high velocity jet where the velocity is too high to allow the flame to stabilize. At the lower inlet velocity of 70 m/s in Fig. 9b, the jet velocity decays more rapidly to a velocity at which the flame can stabilize.

Figure 7 also shows that as the equivalence ratio is increased a regime exists in which, while the flames remain attached, the combustor also becomes quite noisy. This noise consists of a loud, high-pitched whistle in addition to the lower frequency noise associated the high flow rate of reactants out of the inlet nozzle. It is believed that this noise is associated with interactions between the reactant flow in the inlet channels and the flames, which are attached to the channel inlets and, perhaps, burns up into the holes due to the increase in flame velocity with increased equivalence ratio.



**Fig. 9a.** OH PLIF images in confined flame.  $n_{H_2}=1.0$ ,  $u=90$  m/s,  $\Phi =0.33$ .



**Fig. 9b.** OH PLIF images in confined flame.  $n_{H_2}=1.0$ ,  $u=70$  m/s,  $\Phi =0.15$ .

## Summary

The stability and flame characteristics of a premixed, hydrogen-fueled burner were studied. Pure hydrogen and mixtures of hydrogen-blended methane and air were studied. Depending on the inlet flow variables, flame regimes were identified that included both lifted and attached flames. Conditions under which these varying flames were observed were mapped out, as were those conditions at which the flame was extinguished. Generally, the leanest stability limits were found with pure  $H_2$  flames, while the addition of methane required a higher equivalence ratio to maintain a stable flame. At the nominal design conditions for the burner, stable attached flames were achieved. OH PLIF images verified the presence of lifted unattached flames and flame that typically were attached to the burner surface and stabilized in the recirculation/wake region produced by the flow downstream of the solid walls located between reactant inlet channels.

## References

Anderson, D. N., "Effect of Hydrogen Injection on Stability and Emissions of an Experimental Premixed Pre vaporized Propane Burner," NASA TM X-3301, 1975.

Anderson, D. N., "Emissions of Oxides of Nitrogen From an Experimental Premixed-Hydrogen Burner," NASA TM X-3393, 1976.

Barlow, R. S. and Collignon, A., "Linear LIF Measurements of OH in Nonpremixed Methane-Air Flames: When Quenching Corrections Unnecessary," Presented at AIAA Twenty-Ninth Aerospace Sciences Meeting, Reno, NV, January 7-10, paper No. AIAA 91-0179, 1991.

Bell, S. R. and Gupta, M., "Extension of the Lean Operating Limit for Natural Gas Fueling of a Spark Ignited Engine Using Hydrogen Blending," *Combust. Sci. Technol.* **123**: 23-47 (1997).

Clayton, R. M., "Reduction of Gaseous Pollutant Emissions from Gas Turbine Combustors Using Hydrogen-Enriched Jet Fuel – A Progress Report," NASA TM 22-790, 1976.

Gauducheau, J. L., Denet, B. and Searby, G., *Combust. Sci. Technol.* **137**: 81-99 (1998).

Larsen, J. F. and Wallace, J. S., *J. Engineering Gas Turbines and Power* **119**: 218-226 (1997).

Meyers, D. P. and Kubesh, J. T., *J. Engineering Gas Turbines and Power* **119**: 243-249 (1997).

Morris, J. D., Symonds, R. A., Ballard, F. L. and Banti, A., ASME Paper 98-GT-359 (1998).

Nguyen, Q. and Paul, P. H., *Twenty Sixth Symposium (International) on Combustion*, The Combustion Institute, Pittsburgh, 1996, p. 357-364.

Phillips, J. N. and Roby, R. J., ASME Paper 99-GT-115 (1999).

Schefer, R. W., Wicksall, D. M. and Agrawal, A. J., *Twenty-Ninth Symposium (International) on Combustion*, Sapporo, Japan, July 21-26, 2002 (to appear).